HHS Public Access

Author manuscript

Adv Healthc Mater. Author manuscript; available in PMC 2018 January 01.

Published in final edited form as:

Adv Healthc Mater. 2017 January ; 6(1): . doi:10.1002/adhm.201601185.

Substrate Stress-Relaxation Regulates Scaffold Remodeling and Bone Formation *in Vivo*

Max Darnell[a,b], **Simon Young**[a,b], **Luo Gu**[a,b], **Nisarg Shah**[a,b], **Evi Lippens**[c,d], **James Weaver**[b], **Georg Duda**[b,c,d], and **David Mooney**[a,b]

[a]School of Engineering and Applied Sciences, Harvard University, Cambridge, MA 02138

[b]Wyss Institute for Biologically Inspired Engineering, Cambridge, MA 02138

[c]Julius Wolff Institute, Charité—Universitätsmedizin Berlin, 13353 Berlin, Germany

[d]Berlin-Brandenburg Center for Regenerative Therapies, 13353 Berlin, Germany

Abstract

The rate of stress relaxation of adhesion substrates potently regulates cell fate and function in vitro, and here we tested whether it could regulate bone formation *in vivo* by implanting alginate gels with differing rates of stress-relaxation carrying human mesenchymal stem cells into rat calvarial defects. After three months, the rats that received fast-relaxing hydrogels ($t_{1/2} \sim 50s$) showed significantly more new bone growth than those that received slow-relaxing, stiffness-matched hydrogels. Strikingly, substantial bone regeneration resulted from rapidly relaxing hydrogels even in the absence of transplanted cells. Histological analysis revealed that the new bone formed with rapidly relaxing hydrogels was mature and accompanied by extensive matrix remodeling and hydrogel disappearance. This tissue invasion was found to be prominent after just two weeks and the ability of stress relaxation to modulate cell invasion was confirmed with *in vitro* analysis. These results suggest that substrate stress relaxation can mediate scaffold remodeling and thus tissue formation, giving tissue engineers a new parameter for optimizing bone regeneration.

Keywords

Tissue engineering; biomaterials; mechanotransduction; stress relaxation; bone regeneration

Introduction

Biomaterials have been widely explored to promote tissue regeneration, in part due to their ability to tune the extracellular environment surrounding both transplanted and host cells. Tissue engineers have explored a wide array of cues that can be presented to cells, including but not limited to growth factors, drugs, other cell types, extracellular matrix ligands, and mechanical factors (1–4). These efforts seek to improve transplanted cell viability, control cell presence both spatially and temporally, and regulate cell fate decisions, all issues that

Corresponding Author: David Mooney, 29 Oxford St., Cambridge, MA 02138, Phone: (617) 384-9624.

are facilitated with material systems. Despite the broad *in vitro* characterization of the impact of many of these cues on cells, translation of these strategies into the complex *in vivo* milieu has been challenging (5–8).

One set of material cues that has garnered increasing interest is mechanical in nature, involving material properties such as stiffness, porosity, and topography (9, 10). Since it was first shown that adhesion substrate stiffness can influence mesenchymal stem cell differentiation, that observation has been extended to a variety of cell types and outputs, including stem cells of all germ layers and pluripotent stem cells (2, 11). Recently, we, among others, demonstrated that one mechanical property that had been previously ill-explored with regards to its effect on cells, the rate of substrate stress relaxation, is a regulator of cell spreading, proliferation, and osteogenic differentiation of encapsulated mesenchymal stem cells *in vitro*, likely due to an increased ability of cells to remodel the extracellular matrix on these substrates relative to purely elastic substrates (12–15).

This manuscript addresses the hypothesis that substrate stress relaxation can regulate bone regeneration *in vivo*. Bone regeneration could be impacted by the ability of stress relaxation to directly impact osteogenesis, or by the ability of cells to readily remodel and invade rapidly relaxing hydrogels. Cell invasion into implants has previously been shown to be necessary for scaffold-based bone regeneration, motivating past work to design degradability and porosity into engineered implants to allow for cell migration (16). To test our hypothesis, human mesenchymal stem cells (hMSCs) were encapsulated in alginate hydrogels with different stress relaxation time-scales and implanted in rat calvarial defects. To examine the intrinsic ability of rapidly relaxing hydrogels to promote bone regeneration, these gels were also placed in defects without hMSCs. Previous studies have demonstrated the ability of substrate stress relaxation to regulate osteogenic differentiation of mouse mesenchymal stem cells *in vitro* (14), but this effect has not been extended to hMSCs or to an *in vivo* setting. Calcium-crosslinked alginate hydrogels were chosen as cell scaffolds, since alginate has been previously shown to allow for the independent control of initial elastic modulus and stress relaxation time (12, 14). Crosslinking guluronic acid residues on adjacent alginate chains by divalent cations allows for the maintenance of hydrogel microscale architecture independent of crosslinking density and confers viscous damping effects to the hydrogels due to the dynamic nature of the crosslink formation and rupture. Moreover, decreasing the molecular weight of the alginate chains allows for increased chain mobility within the gel mesh and thus a faster relaxation timescale (8, 12, 14). Alginate hydrogels were fabricated at an initial stiffness slightly lower than has been reported to be optimal for osteogenic differentiation of MSCs (17) in order to sensitize the cells to the effect of the stress relaxation and ensure that stiffness effects did not dominate the mechanical cues delivered to the cells. The gels were modified with an RGD peptide motif to support cell adhesion but contained no exogenous growth factors or other soluble factors. A recent study featuring similar hydrogels showed that the pore size and RGD distributions between groups were not significantly different (14). The particular model of bone regeneration was chosen due to its wide use in the field and the possibility of creating a critical-sized defect that does not require external stabilization (18). After explantation, defects that contained implants with relatively fast stress relaxation times showed markedly more bone formation than defects that contained implants with relatively slow stress

relaxation times, as well as extensive matrix remodeling and hydrogel disappearance. Analysis of the early events in this healing process revealed that the fast-relaxing gels are dramatically remodeled within two weeks and *in vitro* studies confirmed that cells are better able to migrate into fast relaxing gels, yielding a new way to control scaffold invasion without the need for engineered chemical degradation or porosity. These results demonstrate that substrate stress relaxation can be a potent parameter for tissue engineers to use to optimize bone regeneration.

Results

We first determined if the native environment of healing bone, the hematoma, would exhibit stress relaxation, to validate the potential physiologic relevance of this parameter for bone regeneration. Human hematomas from adult donors were obtained from the clinic, and subjected to compression testing. These hematomas demonstrated an average relaxation time of ~195 seconds (Fig. 1A), confirming these human tissues demonstrate significant and rapid stress relaxation (Fig. 1A).

Alginate hydrogels were fabricated from either high or low molecular weight polymer to yield distinct rates of stress relaxation, which bracket the rates seen among the hematomas, and their mechanical properties and impact on hMSCs in vitro were first compared. Compression testing confirmed no statistically significant difference in the initial elastic moduli of fast and more slowly relaxing hydrogels (Fig. 1B). As expected, hydrogels fabricated with the high molecular weight alginate demonstrated significantly longer relaxation times than the low molecular weight hydrogels (Fig. 1C). Next, hMSCs were encapsulated in the two types of alginate hydrogels and cultured in osteogenic induction medium for two weeks in order to assess the differences in differentiation of hMSCs in hydrogels with different stress relaxation times. Fast-relaxing gels contracted significantly more than slow-relaxing gels, and, consistent with previous results with mouse stem cells, von Kossa staining of the hydrogels showed significantly more matrix deposition and mineralization for the fast-relaxing hydrogels, indicative of osteogenic differentiation of hMSC (Fig. 1D,E) (14). To confirm the increased mineralization in fast relaxing gels, energy dispersive X-ray spectroscopy (EDS) was performed to map elemental phosphorous in the interior of the hydrogels. Substantially more phosphorous was found in the fast-relaxing gels, consistent with the von Kossa staining, again indicating a greater osteogenic differentiation of hMSCs and subsequent mineral deposition in the fast-relaxing gels (Fig. 1F).

In order to assess the *in vivo* effects of substrate stress relaxation, both types of hydrogels containing hMSCs, as well as an empty defect control and a fast-relaxing hydrogel without cells, were implanted into a rat (RNU rat) critical-sized (8mm) calvarial defect. For the sake of animal welfare, a slow-relaxing hydrogel without cells was omitted, as *in vitro* results suggested that the condition with cells would already perform sub-optimally (19). After three months, the rats were euthanized and the skulls were explanted and examined for bone formation using X-ray micro-computed tomography (μCT). An increase in new bone was found for the fast-relaxing hydrogels, and quantification of the new bone volume confirmed a statistically significant difference in the amount of new bone formed and the average

percentage of the defect that was spanned by bone, when compared to the gels with slower relaxation (Fig. 2). As expected, the empty defects showed minimal bone regeneration, but intriguingly, the fast-relaxing gels without cells showed healing only slightly less than that of the fast-relaxing gels with cells, with this difference not statistically significant (Fig. 2).

The histology of the defects was next examined to assess the structure of the new bone (Figs. 3–4). Masson's Trichrome staining revealed a difference in the thickness of the tissue residing in the defect site, with a nearly two-fold greater thickness in the slow-relaxing case (Fig. 3A–C). In order to gauge the contribution of hydrogel loss to this thickness effect, fast and slow-relaxing hydrogels bearing cells were explanted after two weeks. Safranin O staining for residual alginate showed an intact gel in the slow-relaxing case, but dramatic remodeling and fibrous tissue infiltration with little remaining alginate in the fast-relaxing case (Fig. 3D,E). Hypothesizing that this effect could be due to the ability of surrounding cells to infiltrate the scaffold, an *in vitro* experiment measuring the infiltration depth of fibroblasts initially seeded on top of the gels after one week showed that cells were able to migrate nearly twice as far into the gel in the fast-relaxing case, consistent with the notion that stress-relaxation modulates the ability of cells to remodel and invade a scaffold (Fig. 3F).

H&E, van Gieson, and Masson's Trichrome stainings of three month histology revealed that the new bone formed in the fast-relaxing condition with cells was mature, featuring collagen-rich and relatively acellular regions with sparse osteocytes (Fig. 4A–C). Furthermore, the presence of elongated osteoblasts on the periphery of the new bone, and osteoid regions rich in disorganized collagen suggest active bone growth. In contrast, the slow-relaxing condition showed sparse, disorganized collagen, without prominent bone growth centers or mature bone (Fig. 4A–C). Additionally, Alcian Blue staining for residual alginate revealed little remaining hydrogel in the fast-relaxing case, whereas significant residual hydrogel was noted in the slow-relaxing case (Fig. 4D). Coupled with a significantly larger defect thickness for the slow-relaxing condition, these results confirm that the differences in hydrogel remodeling seen at two weeks are maintained through three months (Fig. 3C, 4D).

In order to gauge the relative contribution of rat versus human cells to the new bone formed in the conditions with transplanted cells, and thus determine the ability of the remodeled scaffold environment to support the viability of transplanted cells, a human mitochondria stain was utilized to label all progeny of the transplanted human cells (Fig. 5). Human cells were markedly absent from the slow-relaxing condition, while a small number of human cells were localized to the periphery of new bone in the fast-relaxing condition (Fig. 5A, B). Quantification of the number of cell nuclei on the perimeter of new bone islands co-localizing with human cells, as a measure of the contribution of the transplanted cells to new bone growth, revealed that 20±11% of cells along the new bone periphery were of human origin (Fig. 5D).

Discussion

These results demonstrate that substrate stress relaxation can be a potent regulator of bone formation *in vivo*. Specifically, rat calvarial defects treated with stiffness-matched hydrogels carrying hMSCs or cell free showed significantly more bone formation after three months if the hydrogels exhibited a relatively fast stress relaxation time. As a recent study showed that substrate stiffness can play an important role in bone regeneration *in vivo* (19), those results combined with those of the present study suggest that substrate stiffness together with the stress relaxation timescale can be tuned to optimize the bone-forming capabilities of biomaterials.

The new bone formed in defects with fast-relaxing implants exhibited a morphology of sparse osteocytes, mineralized matrix and osteoid, indicative of the activation of a robust bone regeneration cascade. Given the complicated material and biological environment of bone, the absence of any of these elements would have suggested that the healing was not taking place in a concerted, directed way. This mature morphology is comparable to the results of previous studies that delivered growth factors such as BMP-2 to defect sites (20), a result that implies a great relative importance of extracellular mechanical properties to bone formation. Based on the apparent potency of both mechanical and biological factors in inducing bone formation, an approach combining mechanical optimization and growth factor delivery, such as one recently reported *in vitro*, could be a promising approach to bone healing in the future (21). That being said, optimizing each approach in perfect isolation may not be possible, as it has been shown that the interaction between soluble factors and biomaterials, and the resulting differences in the mode of factor presentation to cells are potent regulators of cell behavior (22). In this situation, biomaterial systems such as that used in this study that allow for the independent control of key material properties will become increasingly important.

The presence of human-derived cells at the new-bone-periphery in conditions with fast-relaxing gels, but absence of human cells in slow-relaxing conditions indicates a role for fast-relaxing gels in providing survival cues to the transplanted cells as well as a persistent role for the remaining cells in the bone healing cascade. Moreover, the presence of these cells in the zone of new bone formation and not in the mature bone suggests that these cells are actively participating in new bone growth. The same fast-relaxing gels without cells demonstrated slightly less regeneration than with cells, supporting a role of the transplanted human cells in new bone formation. A previous study in which MSCs were encapsulated in alginate hydrogels similar to the slow-relaxing condition here and implanted into subcutaneous pockets in rats reported a marked absence of transplanted cells after just two weeks (23). In contrast, a study in which MSCs were encapsulated in fibrin gels, which are known to demonstrate stress relaxation, and then implanted into a femoral defect model showed significant persistence of the transplanted cells after four weeks (24). The current study suggests stress relaxation as a possible mechanism underlying the discrepancy between the past studies. Additionally, previous work showing the effects of adhesion substrate degradation rate on the ability of transplanted osteoblasts to form bone in an ectopic site could perhaps also be related to effect of stress relaxation, as the mechanisms of stress relaxation and degradation in that study were coupled (25).

This study introduces substrate stress relaxation rate as a key regulator of bone regeneration. Several studies using transplanted MSCs have shown the influence of hydrogel degradation on bone regeneration (26, 27), and the findings here raise the possibility that altered relaxation of the hydrogels as they degrade over time could be contributing to some of the results found in those studies. Additionally, in the early stages of bone fracture healing, periosteal MSCs are known to migrate into the hematoma and participate in intramembranous ossification, differentiating into osteoblasts (28, 29). This study suggests the stress relaxation property of hematomas could mediate both MSC invasion into sites of bone defects and their osteogenic differentiation during bone healing, though such effects are surely mediated by myriad factors such as defect stability and size. Previously, tissue engineers were limited to chemical and biological factor delivery in order to influence bone regeneration, but as the findings of this and another recent study indicate, tissue engineers can leverage the physical properties of biomaterials, in addition to chemical/biological cues, to improve bone regeneration (19).

Materials and Methods

Alginate Hydrogels

Alginate type LF20/40 (FMC Biopolymer) was used as-received (average molecular weight of 280kDa) for the slow-relaxing hydrogels and was irradiated with an 8mRad cobalt source to form the fast-relaxing hydrogels (average molecular weight of 35kDa). Irradiation lowers the molecular weight while maintaining the same G to M block ratio (8). Alginates were modified with GGGGRGDSP peptides (Peptide 2.0) at a ratio of 20 peptides per alginate with standard carbodiimide chemistry as described previously (8). After modification, alginates were dialyzed against a NaCl gradient, treated with activated charcoal, and sterile-filtered. After lyophilization, all alginate was dissolved in serum-free DMEM (Lonza) at 2.5%.

Hydrogels were cast by rapidly mixing the alginate solution with a $CaSO_4$ slurry via two syringes and ejecting the mixture between two glass plates, where it gelled over 1.5 hours. Slow-relaxing gels consisted of 2% LF20/40 alginate and 20mM Ca, while fast relaxing gels consisted of 2% LF20/40 8mRad alginate and 42mM Ca. This difference in calcium concentration has previously been noted to have no effect on mesenchymal stem cell viability and differentiation (14). 8mm disks were then cut from the gel using a biopsy punch.

Hydrogel Mechanical Characterization

Hydrogels were fabricated as described above at a thickness of 2mm and subjected to compression testing using a mechanical testing device (Instron). Gels were compressed at a strain rate of 1mm/min and the Young's Modulus was calculated as the best-fit slope of the first 5–15% of the resulting stress/strain curve. At 15% strain, the strain was held and the time required for the stress to decay by a factor of two was noted.

In Vitro hMSC Differentiation

Human mesenchymal stem cells (Rooster Bio) were encapsulated in slow and fast relaxing hydrogels at a final concentration of 15 million cells/mL gel, gels were punched into disks, and placed into 24-well plates. The encapsulated cells were cultured in osteogenic differentiation medium (Stempro, Life Technologies) and cell culture medium was changed every 3–4 days for two weeks.

At two weeks, samples were fixed in 4% paraformaldehyde for 45 min on an orbital shaker, exposed to increasing concentrations of OCT in a sucrose solution, and flash frozen for cryosectioning. Gels were sectioned at a thickness of 50 μm before von Kossa Staining. Briefly, sections were incubated in a 1% silver nitrate solution under ultraviolet light for 20 seconds, rinsed with DI water, and incubated in 5% sodium thiosulfate for 5 min.

Elemental Analysis of hMSC Differentiation

A Tescan Vega environmental scanning electron microscope (SEM) with a Bruker

XFlash 5030 energy dispersive X-ray spectrometer (EDS) was used for elemental characterization of *in vitro* hMSC differentiation. Gels were prepared in frozen blocks as they were for von Kossa staining and then were sectioned at a thickness of 100 μm onto a p-type silicon wafer. Samples were washed in water, followed by drying under vacuum overnight. Elemental analysis and mapping of phosphorus were performed at an accelerator voltage of 20 keV and a pressure of 12 Pa.

Hydrogel Implantation in Rat Calvarial Defect Model

All animal experiments were performed in compliance with National Institutes of Health guidelines and were approved by the Institutional Animal Care and Use Committee at Harvard University. The rat calvarial defect surgery was performed on four-week old RNU Rats (Charles River Laboratories) as described previously (19). Briefly, animals were anesthetized, and their heads were shaved. A sagittal incision was made along the head and the exposed periosteum was bluntly dissected to the level of the superior temporal line bilaterally. 8mm circular osteotomies were drilled under copious irrigation and the bone removed from the rat calvarium while maintaining the underlying dura intact. 8mm hydrogels encapsulating hMSCs at a density of 10 million cells/mL were implanted into the resulting void. Fascia and skin layers were sutured separately in order to keep the gels stationary.

After two weeks or three months, animals were euthanized with CO_2 and decapitated. The calvarium was removed using bone shears and placed in 10% formalin for 24 hours. Samples were then stored at 4°C in PBS until further use.

X-Ray Micro-Computed Tomography

Rat calvaria were wrapped in paraffin to prevent dehydration and scanned in an X-tek HMXST225 micro-computed tomography system at the Harvard University Center for Nanoscale Systems. Samples were reconstructed using CT Pro and rendered using VG Studio Max software. For new bone quantification in VG Studio Max, an 8mm diameter

cylinder volume of interest was centered over the defect site, with a height equivalent to the thickness of the adjacent bone. The volume within the cylinder encapsulated in an isosurface rendering was calculated, and the percent of defect filled was treated as the fraction of the cylinder, thus representing the original defect volume, filled by the new bone. The spanned fraction was calculated by drawing a line through the center of the defect and calculating the fraction of the original defect diameter that contains bone. The reported maximum fraction is the maximum per animal of all of these lines.

Histology

After tomography, samples were sent to the Dana Farber Cancer Rodent Histopathology Core for paraffin embedding and sectioning, as well as Hematoxylin and Eosin, Van Gieson, Masson's Trichrome, and Alcian Blue staining. Imaging was performed on a Nikon histology microscope. Membrane thickness quantification was obtained by using the measure feature in ImageJ (NIH).

Immunofluorescence staining was performed using anti-human mitochondria primary antibodies (Abcam). Paraffin was removed from sections with two 5 minute xylene washes, and slides were rehydrated in successively lower concentrations of ethanol in DI water. For human mitochondria antigen retrieval, samples were incubated in sodium citrate buffer, pH 6.0, at 95°C for twenty minutes. Slides were blocked in 10% normal goat serum, 1% bovine serum albumin, and 0.05% Tween-20 in PBS for 1 hour at room temperature, and incubated in primary antibody solution using the manufacturer's recommended concentrations overnight at 4°C. Slides were then incubated in goat anti-mouse Alexa 555 secondary antibodies (Abcam) for 1 hour at room temperature and counterstained with Hoescht. Imaging was performed on a Carl Zeiss LSM 710 upright confocal microscope and pseudocolored using ImageJ. Quantification of human cells was obtained in ImageJ by first locating fields of view that previously contained hydrogel, thresholding and binarizing the nuclei, followed by masking the mitochondria channel and counting the masked regions that contained red signal, thus yielding the fraction of nuclei that belonged to human cells. Since human cells were not found outside of these fields, these quantities represent the composition of cells in the neighborhood of the implanted hydrogel.

In Vitro Scaffold Invasion Assay

Slow and fast relaxing hydrogels were fabricated as noted above and were cast on coverslips. Coverslips were placed in wells and NIH 3T3 fibroblasts were seeded at a density of 10,000 cells per square centimeter by pipetting a cell suspension on top of the gels. After twelve hours, the hydrogels were moved to new wells to remove non-adherent cells and the hydrogels were cultured for one week at 37°C. The cells were then fixed with 4% paraformaldehyde for 15 minutes, permeablized with 0.1% Triton X-100 and stained for 15 minutes with rhodamine-tagged phalloidin. The gels were then placed in custom PDMS gaskets on microscope slides and imaged using a Zeiss LSM 710 upright confocal microscope. Z-stacks were captured and the distance from the hydrogel surface to the deepest cell was sampled at five random locations across three different z-stacks using Zeiss ZEN software.

Acknowledgments

The authors would like to thank Christine Cezar for help with immunofluorescence protocols, and Jon Rowley from Rooster Bio for the hMSCs. This work was funded by the NIH/NIDCR (R01 DE013033).

References

1. Huebsch N, Mooney DJ. Inspiration and application in the evolution of biomaterials. Nature. 2009; 462(7272):426–432. [PubMed: 19940912]
2. Murphy WL, McDevitt TC, Engler AJ. Materials as stem cell regulators. Nat Mater. 2014; 13(6): 547–557. [PubMed: 24845994]
3. Mehta M, Schmidt-Bleek K, Duda GN, Mooney DJ. Biomaterial delivery of morphogens to mimic the natural healing cascade in bone. Advanced Drug Delivery Reviews. 2012; 64(12):1257–1276. [PubMed: 22626978]
4. Mooney DJ, Vandenburgh H. Cell Delivery Mechanisms for Tissue Repair. Cell Stem Cell. 2008; 2(3):205–213. [PubMed: 18371446]
5. Szpalski C, Wetterau M, Barr J, Warren SM. Bone Tissue Engineering: Current Strategies and Techniques—Part I: Scaffolds. Tissue Engineering Part B: Reviews. 2011; 18(4):246–257.
6. Mravic M, Péault B, James AW. Current Trends in Bone Tissue Engineering. BioMed Research International. 2014; 2014:865270. [PubMed: 24804256]
7. Smith BD, Grande DA. The current state of scaffolds for musculoskeletal regenerative applications. Nat Rev Rheumatol. 2015; 11(4):213–222. [PubMed: 25776947]
8. Alsberg E, Anderson KW, Albeiruti A, Franceschi RT, Mooney DJ. Cell-interactive Alginate Hydrogels for Bone Tissue Engineering. Journal of Dental Research. 2001; 80(11):2025–2029. [PubMed: 11759015]
9. Hao J, et al. Mechanobiology of mesenchymal stem cells: Perspective into mechanical induction of MSC fate. Acta Biomaterialia. 2015; 20(0):1–9. [PubMed: 25871537]
10. Teo, BKK., Ankam, S., Chan, LY., Yim, EKF. Chapter 11 – Nanotopography/Mechanical Induction of Stem-Cell Differentiation. In: Shivashankar, GV., editor. Methods in Cell Biology. Vol. 98. Academic Press; 2010. p. 241-294.
11. Bellas E, Chen CS. Forms, forces, and stem cell fate. Current Opinion in Cell Biology. 2014; 31(0):92–97. [PubMed: 25269668]
12. Chaudhuri O, et al. Substrate stress relaxation regulates cell spreading. Nat Commun. 2015; 6
13. Cameron AR, Frith JE, Cooper-White JJ. The influence of substrate creep on mesenchymal stem cell behaviour and phenotype. Biomaterials. 2011; 32(26):5979–5993. [PubMed: 21621838]
14. Ovijit Chaudhuri LG, Darinka Klumpers, Max Darnell Sidi A, Bencherif James C, Weaver NH, Hong-pyo Lee, Evi Lippens, Georg N Duda, David J Mooney. Hydrogels with tunable stress relaxation regulate stem cell fate and activity. Nat Materials. 2015; 15:326–334. [PubMed: 26618884]
15. McKinnon DD, Domaille DW, Cha JN, Anseth KS. Biophysically Defined and Cytocompatible Covalently Adaptable Networks as Viscoelastic 3D Cell Culture Systems. Advanced materials (Deerfield Beach, Fla). 2014; 26(6):865–872.
16. Perez RA, Mestres G. Role of pore size and morphology in musculo-skeletal tissue regeneration. Materials Science and Engineering: C. 2016; 61:922–939. [PubMed: 26838923]
17. Huebsch N, et al. Harnessing traction-mediated manipulation of the cell/matrix interface to control stem-cell fate. Nat Mater. 2010; 9(6):518–526. [PubMed: 20418863]
18. Spicer PP, et al. Evaluation of Bone Regeneration Using the Rat Critical Size Calvarial Defect. Nature protocols. 2012; 7(10):1918–1929. [PubMed: 23018195]
19. Huebsch N, et al. Matrix elasticity of void-forming hydrogels controls transplanted-stem-cell-mediated bone formation. Nat Mater. 2015 advance online publication.
20. Haidar Z, Hamdy R, Tabrizian M. Delivery of recombinant bone morphogenetic proteins for bone regeneration and repair. Part A: Current challenges in BMP delivery. Biotechnol Lett. 2009; 31(12):1817–1824. [PubMed: 19690804]

21. Tan S, Fang JY, Yang Z, Nimni ME, Han B. The synergetic effect of hydrogel stiffness and growth factor on osteogenic differentiation. Biomaterials. 2014; 35(20):5294–5306. [PubMed: 24703716]
22. Schultz GS, Wysocki A. Interactions between extracellular matrix and growth factors in wound healing. Wound Repair and Regeneration. 2009; 17(2):153–162. [PubMed: 19320882]
23. Mankani MH, Kuznetsov SA, Wolfe RM, Marshall GW, Robey PG. In Vivo Bone Formation by Human Bone Marrow Stromal Cells: Reconstruction of the Mouse Calvarium and Mandible. STEM CELLS. 2006; 24(9):2140–2149. [PubMed: 16763200]
24. Seebach E, Freischmidt H, Holschbach J, Fellenberg J, Richter W. Mesenchymal stroma cells trigger early attraction of M1 macrophages and endothelial cells into fibrin hydrogels, stimulating long bone healing without long-term engraftment. Acta Biomaterialia. 2014; 10(11):4730–4741. [PubMed: 25058402]
25. Alsberg E, et al. Regulating Bone Formation via Controlled Scaffold Degradation. Journal of Dental Research. 2003; 82(11):903–908. [PubMed: 14578503]
26. Hoffman MD, Xie C, Zhang X, Benoit DSW. The effect of mesenchymal stem cells delivered via hydrogel-based tissue engineered periosteum on bone allograft healing. Biomaterials. 2013; 34(35):8887–8898. [PubMed: 23958029]
27. Hoffman MD, Van Hove AH, Benoit DSW. Degradable hydrogels for spatiotemporal control of mesenchymal stem cells localized at decellularized bone allografts. Acta Biomaterialia. 2014; 10(8):3431–3441. [PubMed: 24751534]
28. Schindeler A, McDonald MM, Bokko P, Little DG. Bone remodeling during fracture repair: The cellular picture. Seminars in Cell & Developmental Biology. 2008; 19(5):459–466. [PubMed: 18692584]
29. Kolar P, et al. The Early Fracture Hematoma and Its Potential Role in Fracture Healing. Tissue Engineering Part B: Reviews. 2010; 16(4):427–434. [PubMed: 20196645]

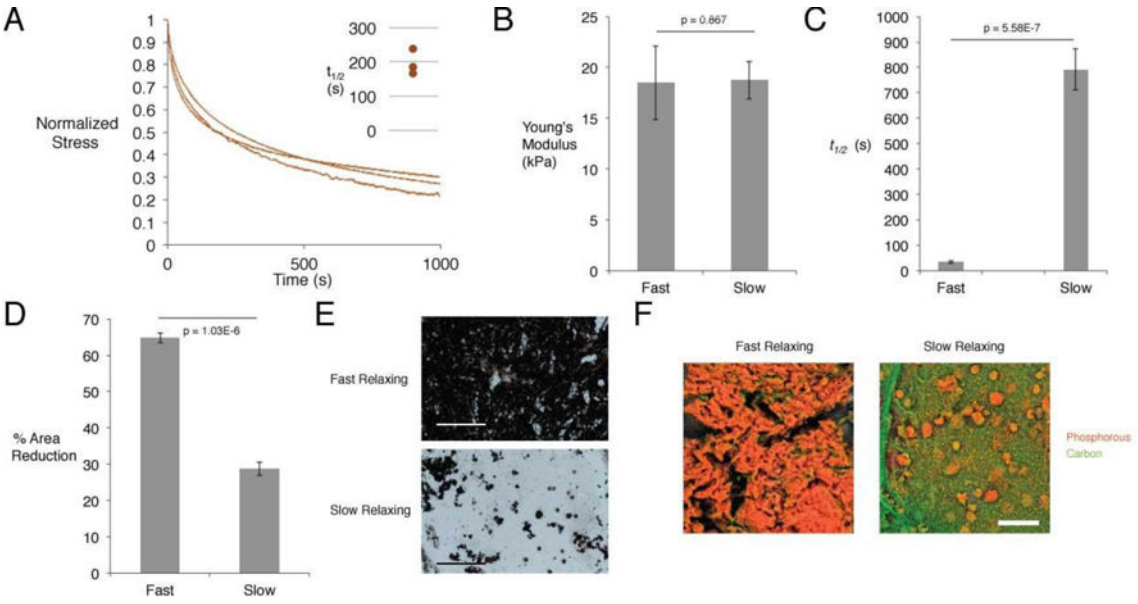

Figure 1.

In vitro characterization of alginate hydrogels, and their effects on hMSC osteogenic differentiation. (A) Stress-time curves of human hematomas subjected to compression testing. Curves depict stress relaxation of hematomas held at 15% strain. Inset shows time to 50% of the initial stress in these curves. (B) Young's modulus as determined by compression testing of slow and fast-relaxing alginate hydrogels. (Student's t-test, n=4) (C) Time to 50% stress relaxation at 15% initial strain for slow and fast-relaxing alginate hydrogels. (Student's t-test, n=4) (D) Extent of gel contraction after culture with encapsulated hMSCs for two weeks. (Student's t-test, n=4) (E) Representative von Kossa staining for matrix mineralization between slow and fast-relaxing gels with encapsulated hMSCs in osteo-inductive medium after two weeks. Scale bar represents 300 μm. (F) Representative pseudo-colored EDS elemental maps for slow and fast-relaxing gels with encapsulated hMSCs in osteo-inductive medium after two weeks. Orange depicts phosphorous and marks phosphate deposition, while green depicts carbon.

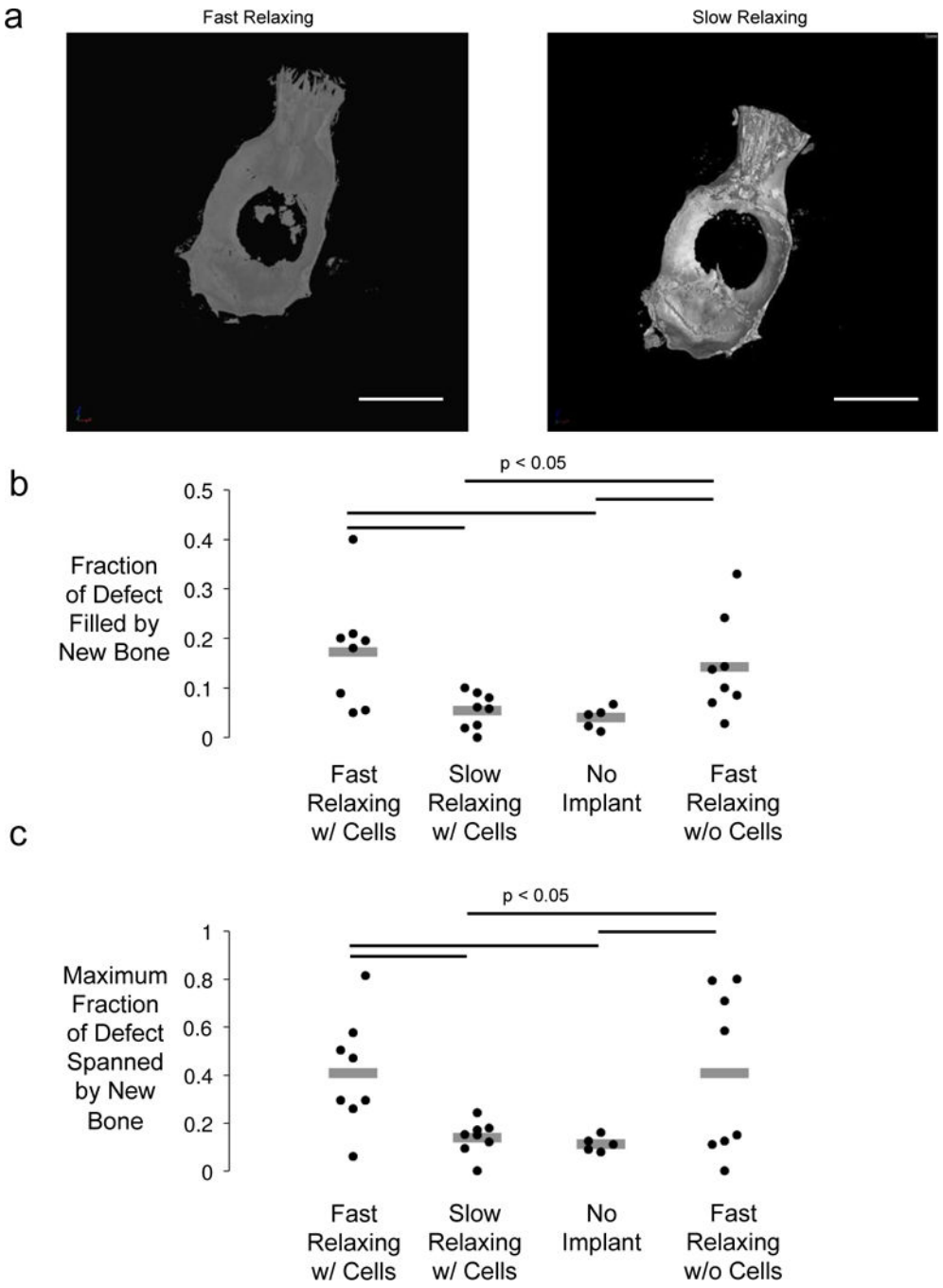

Figure 2.

Micro-computed tomography analysis of new bone formation after implantation of hydrogels in rat calvarial defect model. (A) Representative uCT renderings of rat calvaria three months post-injury. Scale bar – 1cm. (B) Maximum fraction of wound spanned after three months calculated by taking the maximum fraction of bone occupying any line drawn through the center of the defect. (One-way ANOVA, Tukey's post-hoc test, n=3–4) (C) Fraction of the original wound area inhabited by new bone after three months. (One-way ANOVA, Tukey's post-hoc test, n=5–8).

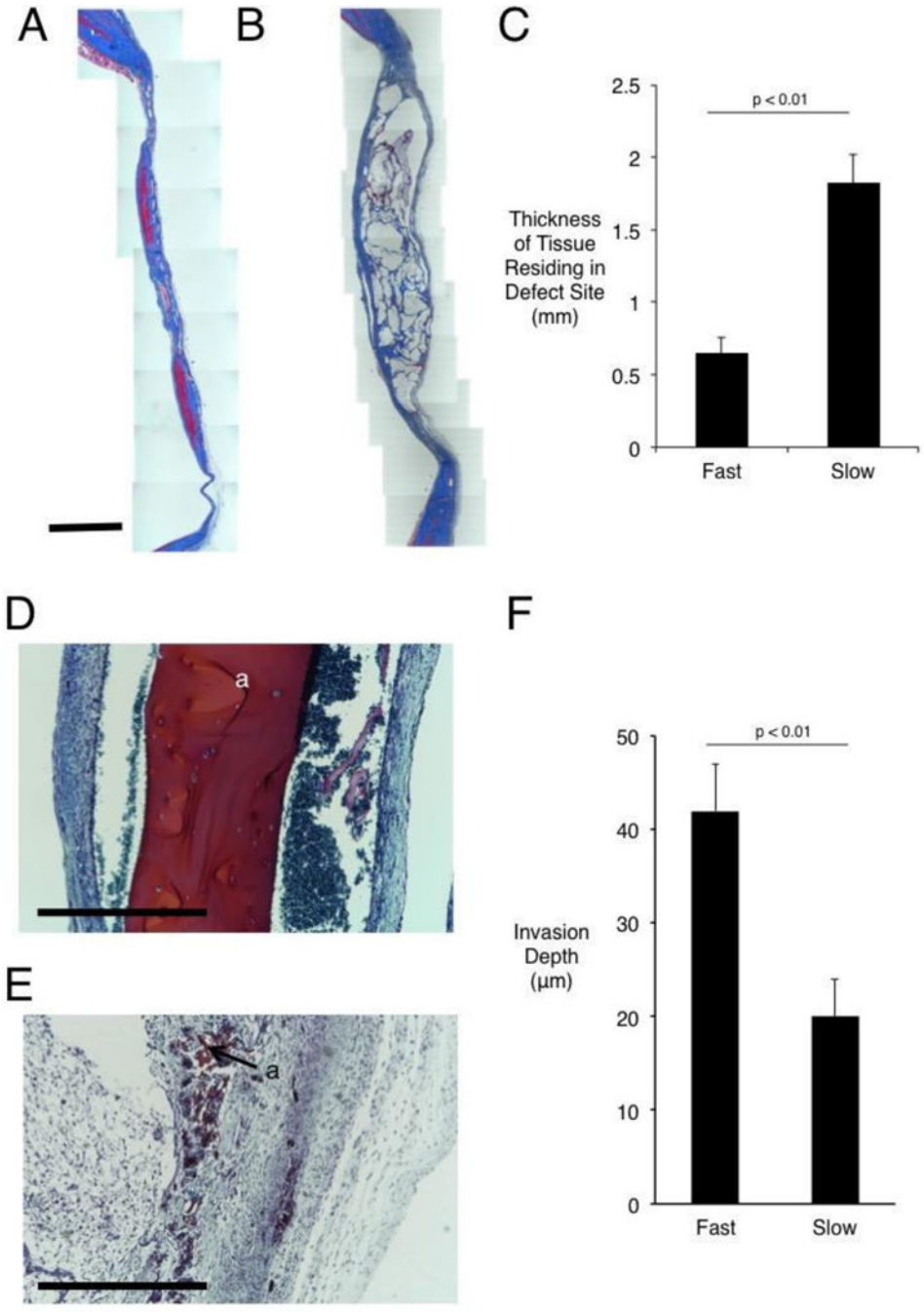

Figure 3.

Histological staining and quantification of calvarial wound site remodeling three months post-injury. (A) Masson's Trichrome staining of defect site in fast-relaxing (A) and slow-relaxing (B) gel conditions. Scale bar – 2mm in A and B. (C) Quantification of thickness of tissue residing in defect site, as determined by measuring tissue sections stained with Masson's Trichrome at various points along the membrane that were incident with the implant (Student's t-test, n=8–10). Error bars represent S.D. (D) Safranin O stain of defect site in slow-relaxing (D) and fast-relaxing (E) cases carrying cells after two weeks of

implantation. Scale bars – 1mm. Residual alginate stains red and is marked “a.” (F) Quantification of fibroblast infiltration into hydrogels at one week *in vitro* after seeding on surface of gel (Student’s t-test, n=15 measurement sites). Error bars represent S.D.

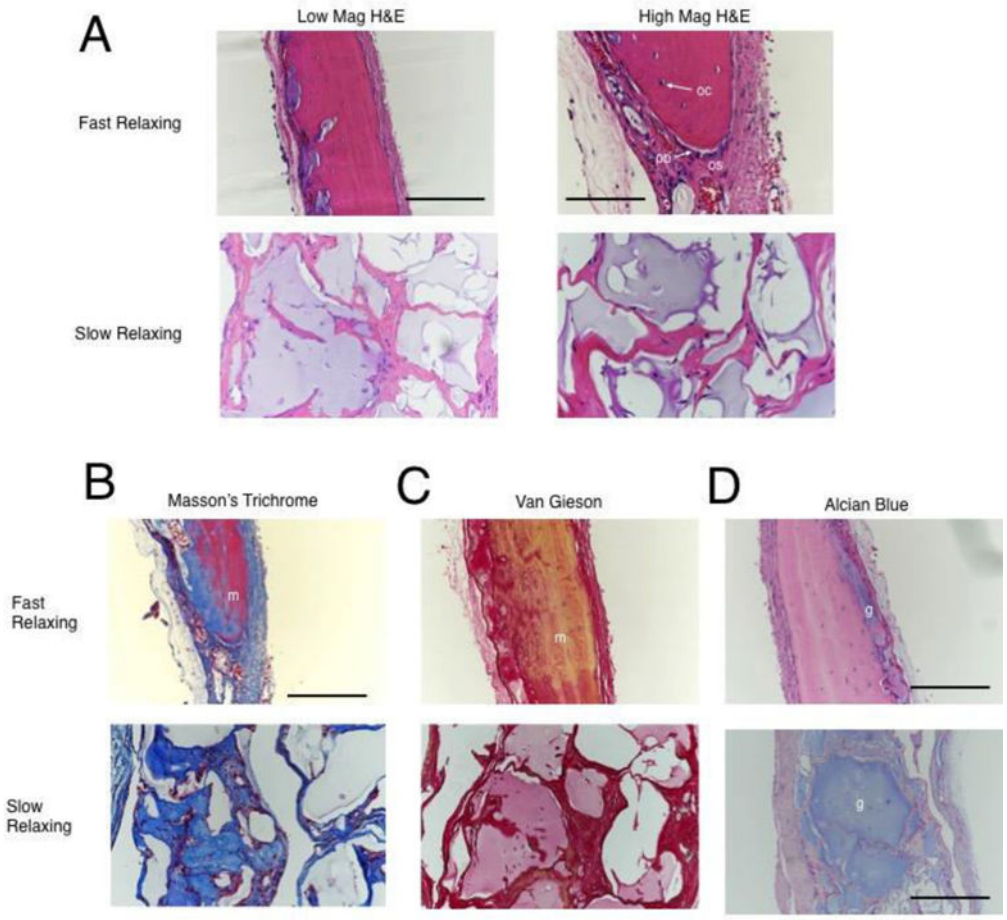

Figure 4.

Histological staining of calvarial wound sites three months post-injury. (A) Representative high and low magnification images of Hematoxylin and Eosin stained sections demonstrating new bone in the fast-relaxing case and a disorganized tissue in the slow-relaxing case. ‘os’ labels the osteoid region, ‘oc’ labels osteocytes, and ‘ob’ labels elongated, activated osteoblasts on the new bone growth front. Low-mag scale bar represents 360 μm and high-mag scale bar represents 180 μm. (B) Representative Masson’s trichrome staining demonstrates mature bone (‘m’) in the fast-relaxing case and disorganized collagen in the slow-relaxing case. Scale bar represents 360 μm. Note the discrepancy in scale due to remodeling effects noted in Figure 3. (C) Representative Van Gieson staining indicates mature bone (‘m’) in the fast-relaxing case and disorganized collagen in the slow-relaxing case. (D) Representative alcian blue staining to identify residual alginate hydrogel (‘g’) reveals small remnants in the fast-relaxing case and large remnants in the slow-relaxing case. Scale bar represents 360 μm in the fast-relaxing case and 720 μm in the slow-relaxing case.

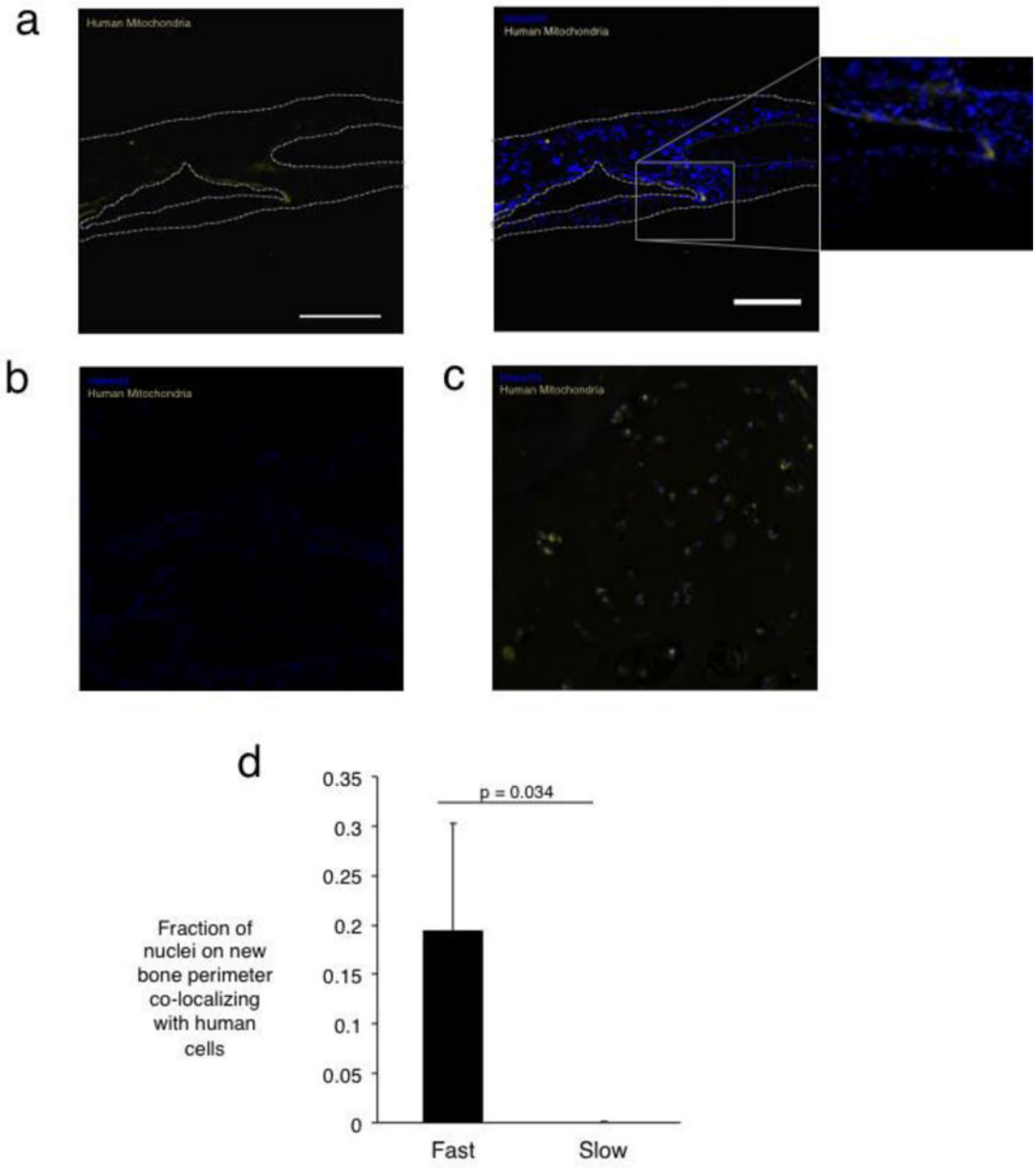

Figure 5.

Localization of progeny of transplanted cells in calvarial defect site three months post-injury. (A) Human mitochondrial staining in defects treated with fast-relaxing gels reveals human cells on the new bone periphery. The left panel depicts imaging of the stain used for human mitochondria, while the right depicts the mitochondria overlaid with nuclei stain. The inset shows a higher magnification version of the new bone interface. Scale bar represents 225 μm (B) Human mitochondrial staining in tissues treated with slow-relaxing gel depicting an absence of human cells. (C) Positive control for human mitochondrial staining in human bone section. (D) Fraction of total cellular nuclei on the new bone perimeter co-localizing

with human cells (Student's t-test, n=4). No human cells were detected in the slow-relaxing case. Error bars represent S.D.